

Monte Carlo wave packet approach to dissociative multiple ionization in diatomic molecules

Henriette Astrup Leth, Lars Bojer Madsen, and Klaus Mølmer

*Lundbeck Foundation Theoretical Center for Quantum System Research, Department of Physics and Astronomy,
Aarhus University, DK-8000 Århus C, Denmark*

(Received 17 February 2010; published 13 May 2010)

A detailed description of the Monte Carlo wave packet technique applied to dissociative multiple ionization of diatomic molecules in short intense laser pulses is presented. The Monte Carlo wave packet technique relies on the Born-Oppenheimer separation of electronic and nuclear dynamics and provides a consistent theoretical framework for treating simultaneously both ionization and dissociation. By simulating the detection of continuum electrons and collapsing the system onto either the neutral, singly ionized or doubly ionized states in every time step the nuclear dynamics can be solved separately for each molecular charge state. Our model circumvents the solution of a multiparticle Schrödinger equation and makes it possible to extract the kinetic energy release spectrum via the Coulomb explosion channel as well as the physical origin of the different structures in the spectrum. The computational effort is restricted and the model is applicable to any molecular system where electronic Born-Oppenheimer curves, dipole moment functions, and ionization rates as a function of nuclear coordinates can be determined.

DOI: [10.1103/PhysRevA.81.053409](https://doi.org/10.1103/PhysRevA.81.053409)

PACS number(s): 33.80.Rv, 42.50.Hz, 31.15.xv

I. INTRODUCTION

When a molecule is exposed to a strong laser pulse the system is excited and ionizes and it starts to dissociate. For intense pulses of interest in current experiments, for example, wave lengths ~ 800 nm, peak intensities $\sim 10^{14}$ W/cm², and durations in the femtosecond regime, all these processes are, in principle, accurately described by the time-dependent Schrödinger equation (TDSE). The dynamics introduced by the external field, however, is so strong that the solution of this equation including all degrees of freedom is impossible even for H₂, and modeling has accordingly focused separately on either electronic ionization or nuclear dissociation dynamics.

In the existing modeling of strong-field dissociative double ionization of the simplest neutral molecule, H₂, it is assumed that one of the electrons is removed early in the pulse [1–4]. In the parallel geometry, full *ab initio* calculations are then possible for the remaining part of the pulse [5] and in this way a high degree of agreement with experiments may be achieved. However, the method still treats the first ionization in an *ad hoc* manner and gives only a little hope for extensions to larger molecular systems. Simpler models have been proposed to fulfill the desire of potential extensions. Using the Born-Oppenheimer (BO) approximation, and including only the two lowest electronic states patterns in the kinetic-energy release (KER) spectrum were reproduced for certain pulse parameters [1,6]. Experiments also exist using H₂⁺ from ion sources [7–9], and an understanding of some features of the KER spectra was obtained in terms of a Floquet picture [9].

The purpose of the present work is to give a detailed description of the Monte Carlo wave packet (MCWP) technique, which we recently introduced for the description of dissociative multiple ionization by an intense near-infrared laser pulse in [10]. The technique provides a consistent theoretical framework that accounts for both ionization and dissociation dynamics, and is applicable to any molecular system where electronic structure, dipole moment functions, and ionization rates as a function of internuclear coordinates can be determined. As an example, illustrating the methodology and

calculations in a particular case, we study double ionization of H₂ using pulses of 800 nm, 40 fs, and 1×10^{14} W/cm². From the example it is clear that including many different times for the first ionization event as well as many intensity components of the field is very important. In a sequel to this paper [11], several other experiments on D₂ as well as H₂ are discussed.

Based on the BO approximation we start in the electronic and nuclear ground state of H₂ and study the nuclear dynamics as the population is transferred to states of H₂⁺ and subsequently ionized leading to Coulomb explosion. This is done by treating both ionization steps as decay processes, incorporated in a master equation for the molecular density matrix. By this approach we benefit from the explicit separation of the fast electronic dynamics from the nuclear dynamics, and within the validity of our model, a consistent separation of the multichannel problem into different ionization stages. The MCWP technique was first introduced for dissipative processes in quantum optics [12–14], and has later been used for example in molecular physics [15,16]. In numerous studies [14,17–21], the method has been used to replace the solution of the density matrix master equation by the solution of stochastic Schrödinger equations for an ensemble of wave functions. The ensemble simulations are considerably easier when the Hilbert space dimension N is large and the number of density matrix elements N^2 is very large.

The paper is organized as follows. First Sec. II gives a brief summary of how density matrices and the master equation are used in quantum optics to solve interacting quantum systems (Sec. II A) and how this can be applied to study ionization events as well (Sec. II B). This constitutes background material for Sec. III, where the MCWP technique is introduced as a method to simulate the master equation (Sec. III A). As shown in Sec. III B, the MCWP approach can also be derived directly from the dynamics of the molecule, conditioned on the simulated detection of electrons escaping the molecule at random instants of time. Up to this point, the discussion is general, however, in Sec. IV we turn to study dissociative double ionization of H₂ as a special

example, including first a derivation of the Hamilton operator (Sec. IV A) and the jump operators (Sec. IV B) followed by a discussion of the calculational strategy (Sec. IV C). In Sec. V we show how different elements of the MCWP method come into play in addressing this problem and account for the agreement between our calculations and experiments. Section VI concludes the paper.

Atomic units ($\hbar = m_e = e = 1$) are used throughout this paper unless stated otherwise.

II. DENSITY MATRIX AND MASTER EQUATION APPROACH TO DISSOCIATIVE DOUBLE IONIZATION

The conventional TDSE describes the evolution of an isolated quantum system or a quantum system driven by an external interaction, which can be parameterized by an operator $\hat{V}(t)$ acting on only the quantum mechanical degrees of freedom of the system of interest. Interacting particles that form composite quantum systems are in the same way described by the TDSE, which now has to be solved for a state vector in the tensor product Hilbert space. Except for specific cases, such a TDSE calculation is, in practice, so complicated that it prevents exact quantum mechanical calculations and very good approximations have been established to deal with different interesting cases. One of these cases includes a single quantum system interacting weakly with an environment, whose properties permit an effective replacement of the full system-environment dynamics by an effective description of the system alone. The evolution is no longer unitary, and if energy is dissipated irreversibly into the environment, one can introduce decay and decoherence rates and solve a so-called master equation for the density matrix of the smaller quantum system of interest.

The purpose of the present section is first to recapitulate the density matrix approach to dissipative processes in quantum optics, where photon emission (e.g., by an atom) is described by rate equation terms in a master equation (Sec. II A), and second to describe in an equivalent manner the situation where electrons leave a molecular system (Sec II B).

A. The quantum optical master equation

A key example of the approximate solution of interacting quantum systems is the Weisskopf-Wigner approach [22] to spontaneous atomic decay, where an excited atom decays into low-lying electronic states by emission of light. Treating the atom as the small system, the environment is here defined as the quantized electromagnetic radiation field occupying space around the atom. The coupling between the two systems is the usual minimal coupling between charges and radiation, where the radiation field is expressed in terms of field operators, which lead to the creation and destruction of photons (e.g., in traveling wave field modes). The TDSE for the composite system can be used to propagate the quantum amplitudes on the atomic excited state (with no photons) and on the various states of the field with a single photon populating light modes propagating in different directions in space (leaving a ground-state atom behind). The state vector of the composite system has infinitely many amplitudes associated with the wave vectors and polarization of the emitted photons, but to an

excellent approximation, the total population of all these states grows according to a simple rate process, and the coupling precisely accounts for the atomic decay rate.

If the atom also interacts with a laser field, as represented by a coherent coupling between the ground and excited states, it may become re-excited and emit photons several times, and thus populate states of the environment with multiple photons present. This exploration of larger and larger photon number components of the Hilbert space makes the solution of the full TDSE impossible. It is possible, however, to combine the rate equations and the coherent atomic dynamics in the master equation for the atomic density matrix $\sigma(t)$ [21],

$$\frac{d}{dt}\sigma(t) = i[\sigma(t), H_s] + \mathcal{L}_{\text{relax}}(\sigma(t)), \quad (1)$$

where σ is an operator on the reduced Hilbert space of the isolated atom, and where H_s , acting on the same space, includes the Hamiltonian of the isolated atom and its interaction with the classical laser field. The commutator term is fully equivalent to the Schrödinger equation evolution of the state vector of an isolated system. The relaxation term, $\mathcal{L}_{\text{relax}}(\sigma(t))$, includes the rate equations for the atomic populations and coherences, the diagonal and off-diagonal elements of σ , respectively.

It has been proven, that a linear, continuous differential equation for the density matrix has to be of so-called Lindblad form, if the density matrix must retain its physical properties as a density matrix of a quantum system [21].

This canonical form of the relaxation superoperator, $\mathcal{L}_{\text{relax}}(\sigma(t))$ is parameterized as [21]

$$\begin{aligned} \mathcal{L}_{\text{relax}}(\sigma(t)) = & -\frac{1}{2} \sum_m [C_m^\dagger C_m \sigma(t) + \sigma(t) C_m^\dagger C_m] \\ & + \sum_m C_m \sigma(t) C_m^\dagger, \end{aligned} \quad (2)$$

where the operators C_m have dimension of (time)^{-1/2}. In case of a two-level quantum system that decays with the rate Γ from its excited to its ground state, $|e\rangle \rightarrow |g\rangle$, the master equation contains a single C_m operator, $C = \sqrt{\Gamma}|g\rangle\langle e|$, while more complicated problems employ several C_m operators to account for branching ratios between different decay channels.

For an atom with only two coupled states, the corresponding 2×2 density matrix has only four elements, and the master equation, Eq. (1), is readily solved and provides the values of these four elements and hence also the expectation value of any atomic observable as a function of time.

Although the field is formally eliminated from the description, and its intensity, spectral distribution, and so on, have to be inferred by a subsequent analysis, we may formally represent the density matrix as a sum [20,23],

$$\sigma(t) = \sum_n \sigma^{(n)}(t), \quad (3)$$

where each term $\sigma^{(n)}(t)$ represents the atomic state associated with the component of the full quantum state with exactly n photons present in the quantized radiation field. The ground-state population of $\sigma^{(n)}$ is fed by the atomic decay rate from the excited-state component of $\sigma^{(n-1)}$, and the master equation,

Eq. (1), can be directly interpreted as the result of summing up the full set of coupled equations for the individual $\sigma^{(n)}$'s,

$$\frac{d}{dt}\sigma^{(n)}(t) = i[\sigma^{(n)}(t), H_s] + \mathfrak{L}_{\text{loss}}(\sigma^{(n)}(t)) + \mathfrak{L}_{\text{feed}}(\sigma^{(n-1)}(t)) \quad (4)$$

where the relaxation terms are now separated in a loss term and a feeding term. For the spontaneous emission problem, the two terms correspond precisely to the first and second sums in (2), respectively. For continuous laser irradiation, terms with larger and larger values of n become significant with time, illustrating the associated computational challenge.

B. Dissociative ionization as a system-reservoir problem

In this work we present a formulation of dissociative ionization of molecules as a system-environment interaction problem, and we establish a master equation for the molecule or molecular ion along the same lines as the quantum optical master equation for the light-emitting atom. The environment is the space around the molecule, which is initially empty, but due to ionization it becomes populated with electrons in every ionization step, analogous to the creation of photons in the light-emission problem in quantum optics (see the discussion in Sec. II A). It is a significant difference between the quantum optics and ionization problems that the light-emitting atom is left intact, and hence the atomic $\sigma^{(n)}$'s associated with different numbers of emitted photons in (3) and (4) are all density matrices on the same Hilbert space, while the emission of an electron from the molecule leaves the molecule in an ionized state belonging to an entirely different Hilbert space. This physical difference, however, does not invalidate Eq. (3) and its probabilistic interpretation of the density matrix as a statistical mixture of different possible states, which in the current case includes different charge states of the quantum system.

The formal identification of our problem with a system and an environment component does not imply the validity of a master equation of the form given in Eq. (1), and the derivation of the Weisskopf-Wigner theory of spontaneous emission, indeed, contains a delicate analysis of the system-environment interaction. This analysis is often referred to as the Born-Markov approximation [18,20] to signal that the interaction is weak and thus treated by perturbation theory, while the environment is Markovian (i.e., a quantum excitation of the environment degrees of freedom spreads rapidly and previously dissipated excitations are not re-absorbed by the small quantum system at later times). Mathematically, this spreading occurs if the environment supports a wide band of states so that a superposition of energy eigenstates, formed at a given time t , has rapidly evolving relative phases between different components which destroys its coherent coupling to the small system already shortly after the emergence of an excitation in the environment. In the Weisskopf-Wigner theory, this mathematical dephasing is caused by the energy spread of photon states with different wave numbers, which in turn is equivalent to the physical argument that photon wave packets propagate away from the emitter at the speed of light. The weakness of the system-environment coupling ensures that the photon indeed travels far away from the atom and is irretrievably lost during the emission process.

To apply a similar description for the ionization process, we thus assume that the ionized continuum electrons are released and leave the molecular ion so fast that re-absorption does not occur. The separation of time scales is not as favorable as in the optical case, and some TDSE calculations of atomic and molecular ionization [24–26], indeed, show a short time oscillatory behavior rather than a linear monotonous increase in the ionization probability. These short transients, however, have only low probability weight, and the dominant ionization is compatible with a rate process. The very convincing agreement between the present theory and experiment (see also [10,11]) shows that this assumption is well justified for a range of laser parameters used in recent strong-field dissociative ionization studies and we shall hence assume the validity of the master equation model of the ionization process.

III. MONTE CARLO WAVE PACKET THEORY

The density matrix is an operator on the system Hilbert space characterized by a number of variables which is the square of the Hilbert space dimension used to represent the quantum system. For few-level systems, the master equation, Eq. (1), is thus readily solved, but for problems with a large Hilbert space, such as spatial motion, the solution of the master equation may present a formidable task, even though the environment degrees of freedom have disappeared from the formalism. For these problems, it is useful to apply the MCWP technique, which replaces the density matrix by an ensemble of individual state vectors which are evolved stochastically with time [12–14]. In this section we will give a basic introduction to this method and explain its functioning for the ionization problem.

A. Formal equivalence of master equation and stochastic wave-function solutions

As shown in [18], a master equation with relaxation terms of the form given in Eq. (2) can be simulated by propagating an ensemble of pure-state wave functions subject to a non-Hermitian Hamilton operator

$$H = H_s - \frac{i}{2} \sum_m C_m^\dagger C_m, \quad (5)$$

where H_s is the Hamiltonian without the relaxation terms and C_m are the Lindblad relaxation operators. Additionally, random jump events are included. The jump events between states of the system are implemented as follows: Due to the non-Hermitian correction to the Hamiltonian, it does not conserve the norm of the wave function when it is propagated in time. In each time step, the reduction in norm dP provides the probability that the wave function is subject to a quantum jump process. These jump processes are implemented as the action of one of the operators C_m on the wave function. To simulate the jumps with the desired probabilities, a random number generator is used, and the following operations have to be performed for every wave function and in every time step during the evolution of the system:

1. Propagate the quantum state $|\Psi(t)\rangle$ of the system using the non-Hermitian Hamiltonian H

$$|\tilde{\Psi}(t + dt)\rangle = \exp(-iHdt)|\Psi(t)\rangle, \quad (6)$$

where it is assumed that dt is so small that H can be considered constant over this time interval.

2. Determine the reduction in norm dP of the propagated state

$$dP = 1 - \langle \tilde{\Psi}(t+dt) | \tilde{\Psi}(t+dt) \rangle. \quad (7)$$

In the case of a several Lindblad relaxation operators C_m , we have to first order in dt

$$dP = \sum_m dP_m \equiv \sum_m \langle \Psi(t) | C_m^\dagger C_m | \Psi(t) \rangle dt. \quad (8)$$

3. Make a probabilistic decision, whether the system is subject to a quantum jump (probability dP) or not (probability $1 - dP$): Pick a random number ϵ uniformly distributed between zero and unity.

3a. If $\epsilon > dP$: No transition occurs and the wave function $|\tilde{\Psi}(t+dt)\rangle$ is renormalized

$$|\Psi(t+dt)\rangle = \frac{1}{\sqrt{1-dP}} |\tilde{\Psi}(t+dt)\rangle. \quad (9)$$

3b. If $\epsilon < dP$. A transition occurs by application of one of the ‘‘quantum jump’’ operators C_m , picked at random according to their relative weights/branching ratios dP_m/dP ,

$$|\Psi(t+dt)\rangle = N_n C_n |\Psi(t)\rangle, \quad (10)$$

where $N_n = 1/\sqrt{dP_n/dt}$ is the appropriate normalization constant.

4. Return to point 1 for the next time step.

The equivalence between the master equation and the average over a large number of stochastic wave functions can be explicitly demonstrated by averaging the statistical operator $\sigma(t+dt) = |\Psi(t+dt)\rangle\langle\Psi(t+dt)|$ over the outcomes of the stochastic procedure just outlined. Using that at time $t+dt$ the system with probability $(1-dP)$ is in the renormalized state $|\tilde{\Psi}(t+dt)\rangle/\sqrt{1-dP}$ and with probability dP_n occupies the state $C_n|\Psi(t)\rangle/\sqrt{dP_n/dt}$, one readily obtains the weighted-average evolved state [14]

$$\begin{aligned} \overline{\sigma(t+dt)} &= (1-dP) \times \frac{|\tilde{\Psi}(t+dt)\rangle\langle\tilde{\Psi}(t+dt)|}{1-dP} \\ &+ \sum_n dP_n \frac{C_n|\Psi(t)\rangle\langle\Psi(t)|C_n^\dagger}{dP_n/dt} \\ &= \sigma(t) + idt[\sigma(t), H_s] + dt\mathcal{L}_{\text{relax}}(\sigma(t)). \end{aligned} \quad (11)$$

Using the linearity of this equation, we can similarly provide the time evolution of the average of $|\Psi\rangle\langle\Psi|$ for an ensemble which already at time t constitutes a mixed state $\overline{\sigma}(t)$,

$$\frac{d\overline{\sigma}(t)}{dt} = i[\overline{\sigma}(t), H_s] + \mathcal{L}_{\text{relax}}(\overline{\sigma}(t)). \quad (12)$$

This linear equation is identical to the master equation (1), and we therefore conclude that the statistical average evolution of the ensemble state vectors reproduces the master equation solution for the density matrix.

B. Physical meaning of stochastic wave functions

The stochastic wave functions are not only a computational trick to simulate the density matrix evolution. They can be obtained directly from the system-environment problem, and

in this way, via Eq. (11), they offer an alternative derivation of the master equation itself. In our simple example (Sec. II A) with an atom that decays by spontaneous emission, the full quantum description uses as an initial state an atomic state atom with no photons present. In the course of the system-environment interaction, the system evolves continuously into a modified atomic state and no photons, plus a component with the atomic ground state and a single photon present. If the ground-state atom is re-excited by a laser field, more and more state vector components appear with also 2, 3, and more photons present in the environment. At this stage atomic observables are accounted for by the atomic density matrix, which can be interpreted as an incoherent sum of the terms with the different photon number components given in Eq. (4). Instead of obtaining this atomic state as a weighted sum over all possible components with different photon number in the environment, one may simulate the effect of measurements of the photon number and thus at every time-step project the state of the field and choose the associated atomic-state component according to the random outcome of the measurement.

This idea rests on the validity of the Born-Markov approximation [18,20] (i.e., that photons that were previously dissipated into the environment are not coming back to affect the future evolution of the system). Any physical process applied to them, including measurements, should hence not change the average dynamics of the system.

We now come to the simulation of dissociative multiple ionization of molecular systems. Here, the environment is associated with the electrons escaping the molecular ion, and the hypothetical measurement of these electrons effectively removes them from the quantum description and projects the remaining molecular system on the charge state corresponding to the measurement outcome. The Born-Markov approximation limits the method to processes where the recapture of liberated electrons is not a significant component of the dynamics. In comparison with the quantum optical case, we do not only change state, but we also change the physical system whenever an electron is detected. However, as we shall see in the following, we still have a definite procedure to deduce a pure quantum state at all times during time evolution.

We conclude this section by emphasizing that the equivalence between the simulated average outcome and the master equation is a mathematical result, which holds irrespective of the formal correspondence between the random elements in the procedure and an idealized measurement procedure. The MCWP simulations make physical predictions also for experiments, where the electrons are not being measured.

IV. DISSOCIATIVE DOUBLE IONIZATION OF H₂

Having introduced the MCWP technique, we now apply the method to dissociative double ionization of H₂ in short intense laser pulses. Based on the BO approximation, the electronic and nuclear degrees of freedom are separated and an overview of the dissociative ionization process is given in Fig. 1. Starting in the ground state of H₂, only one electronic state is included, namely $(1s\sigma_g)^2$ and the system is propagated in this state until the first quantum jump (i.e., until the imaginary electron detector measures one emitted electron). The nuclear wave function is then instantaneously transferred to the H₂⁺

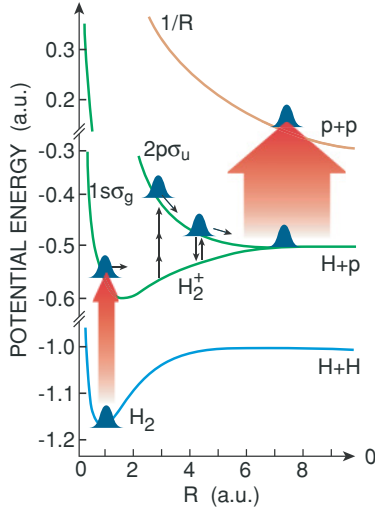


FIG. 1. (Color online) Illustration of the four field-free Born-Oppenheimer potential energy curves used in the present MCWP description of dissociative double ionization of H_2 . During the ionizing pulse the wave packet is transferred from the neutral to the singly ionized, and further to the doubly ionized state. Both transitions occur at a specific time, however, calculations using all possible jump times are made and only upon averaging the correct physical picture is obtained (see the discussion in Sec. IV).

system. For the singly ionized molecule, two electronic states are included, the bonding $1s\sigma_g$ state and the dissociative $2p\sigma_u$ state, and until the detection of a second electron the system evolves on these coupled electronic states. At the time of the second detection, the system is subjected to a second quantum jump and the nuclear wave function is transferred to the final Hilbert space. Here only two protons are present and the absence of electrons leads to an effective $1/R$ potential due to the nuclear repulsion. The approach is straightforwardly extended to include more states such as the autoionizing states of H_2 . The four electronic states mentioned here, however, are sufficient to illustrate the method and to obtain very good agreement with many experiments (see Fig. 7 and [11]).

A. The Hamilton operator

To quantify the MCWP approach to dissociative double ionization of H_2 , the non-Hermitian operator, Eq. (5), is first to be determined. This operator contains both a relaxation term and a Hermitian part H_s . The latter is the system Hamiltonian leaving out interactions that induce transitions among the different charge states. This operator can be separated into three terms

$$H_s = T_{\text{nuc}} + L_{\text{elec}} + H_{\text{elec}}. \quad (13)$$

The kinetic-energy operator of the nuclei is here denoted T_{nuc} , the coupling of the electrons to the external field is denoted L_{elec} and the remaining terms including electronic kinetic energy and electrostatic interaction is contained in the electronic Hamiltonian H_{elec} . Having made this separation we adapt the BO approximation and study the nuclear evolution in a basis of electronic states, $|\phi_{Ra}\rangle$, fulfilling

$$H_{\text{elec}}(R)|\phi_{Ra}\rangle = E_a(R)|\phi_{Ra}\rangle. \quad (14)$$

The solutions depend on both the energy E_a for the electronic state a and the internuclear separation R . Even though there are infinitely many electronic states, we only include four in the present example. These are $(1s\sigma_g)^2$ in H_2 , $1s\sigma_g$ and $2p\sigma_u$ in H_2^+ , and the doubly ionized state H_2^{++} , for short denoted h , g , u , and c , respectively. The total state ket $|\Psi\rangle$ is now expanded in these four orthonormal states

$$|\Psi\rangle = \sum_a \int d\vec{R} X_a(\vec{R}, t) |\phi_{Ra}\rangle \otimes |\vec{R}\rangle, \quad (15)$$

where the prefactors $X_a(\vec{R}, t)$ are the nuclear wave functions, $|\vec{R}\rangle$ the position eigenkets of the nuclear coordinate, and $a = \{h, g, u, c\}$ the different electronic states.

To derive the equations of motion for the nuclear wave functions, we turn to the time-dependent Schrödinger equation $i \frac{d}{dt} |\Psi\rangle = H_s |\Psi\rangle$. Inserting Eq. (15), projecting on both sides with $\langle R' | \otimes \langle \phi_{R'a'} |$ and using that the Hamiltonian is local in space, we obtain

$$i \frac{d}{dt} X_{a'}(\vec{R}', t) = \sum_a \int d\vec{R} \delta(\vec{R}' - \vec{R}) \langle \phi_{R'a'} | H_s X_a(\vec{R}, t) | \phi_{Ra} \rangle. \quad (16)$$

The matrix element on the right-hand side contains three terms due to the separation of H_s in Eq. (13). The matrix elements of H_{elec} give a delta function in a and a' and the known electronic energies E_a [27].

$$\langle \phi_{R'a'} | H_{\text{elec}} X_a(\vec{R}, t) | \phi_{Ra} \rangle = \delta_{a'a} X_a(\vec{R}, t) E_a(R). \quad (17)$$

Turning to the electron-field interaction, the length gauge is adapted and the coupling between an electron at position \vec{q}_j and the external field \vec{F} takes the form $\vec{q}_j \cdot \vec{F}$.

$$\begin{aligned} \langle \phi_{R'a'} | L_{\text{elec}} X_a(\vec{R}, t) | \phi_{Ra} \rangle \\ = |F| \cos \theta_0 \sum_{j=1,2} \langle \phi_{R'a'} | q_j | \phi_{Ra} \rangle X_a(\vec{R}, t), \end{aligned} \quad (18)$$

where θ_0 denotes the angle between the field polarization and the internuclear vector \vec{R} . In the following, rotation of the molecule is neglected, since the characteristic time scale is on the order of 170 fs and θ_0 is approximately constant for each molecule during the shorter pump pulse (see [28] for a recent detailed discussion of this axial recoil approximation). Evaluation of $\langle \phi_{R'a'} | q_j | \phi_{Ra} \rangle$ should, in principle, be done for all combinations of a and a' . However, since only terms in the Hamiltonian not responsible for coupling among different Hilbert spaces are of concern, just a single term $\langle \phi_{Rg} | q_j | \phi_{Ru} \rangle$ and its complex conjugate survive [27].

The last term to evaluate is the matrix element concerning the kinetic energy of the nuclear motion $T_{\text{nuc}} = \frac{1}{2\mu} \vec{P}_{\vec{R}}^2$, where μ is the reduced mass of the nuclei and $\vec{P}_{\vec{R}} = -i \nabla_{\vec{R}}$ is the momentum operator of the relative coordinate \vec{R} . In writing out the operator, the neglect of rotations during the pulse in combination with the BO approximation gives

$$\langle \phi_{R'a'} | T_{\text{nuc}} X_a(\vec{R}, t) | \phi_{Ra} \rangle = -\delta_{a'a} \frac{1}{2\mu} \frac{1}{R} \frac{\partial^2}{\partial R^2} R X_a(\vec{R}, t). \quad (19)$$

Additionally, the nuclear wave function can be expressed as

$$X_a(\vec{R}, t) = \frac{1}{R} K_a(R, t) W_{\theta_0, \phi_0}(\theta, \phi), \quad (20)$$

with $W_{\theta_0, \phi_0}(\theta, \phi)$ specifying a tight static internuclear orientation along polar angles θ_0, ϕ_0 .

Using the above matrix elements in combination with Eq. (16) and the time-dependent Schrödinger equation, the Hermitian part of the Hamiltonian becomes

$$\begin{aligned} H_s = & \sum_a \int d\vec{R} \left[-\frac{1}{2\mu} \frac{1}{R} \frac{\partial^2}{\partial R^2} R + E_a \right] |\phi_{Ra}\rangle \langle \phi_{Ra}| \otimes |\vec{R}\rangle \langle \vec{R}| \\ & - |F| \cos \theta_0 \int d\vec{R} \langle \phi_{Rg} | q_j | \phi_{Ru} \rangle [|\phi_{Rg}\rangle \langle \phi_{Ru}| \\ & + |\phi_{Ru}\rangle \langle \phi_{Rg}|] \otimes |\vec{R}\rangle \langle \vec{R}|. \end{aligned} \quad (21)$$

B. The jump operators

The non-Hermitian part responsible for the jumps among the different Hilbert spaces is now to be determined. All electronic transitions are assumed to be vertical in Fig. 1, i.e., to occur without displacement or recoil of the nuclear motion. The transition jump operator responsible for the first ionization, bringing population from the ground state in H_2 to the lowest state in H_2^+ , is local in the nuclear coordinate and reads

$$C_h = \int d\vec{R} \sqrt{\Gamma_h(\vec{R})} |\phi_{R,g}\rangle \langle \phi_{R,h}| \otimes |\vec{R}\rangle \langle \vec{R}|. \quad (22)$$

In this paper the static field rates $\Gamma_h(\vec{R})$ calculated for H_2 in Ref. [29] were used as instantaneous ionization rates changing in every time step according to the current strength of the oscillating external field. No overall phase is included since the different contributions to the final KER spectrum are added incoherently and hence independent on the relative phase of the nuclear wave functions in the different evolutions of the system.

The jump operator C_h represents a transition from the ground state in H_2 to the lowest field-free state in H_2^+ . As the ionization occurs during the pulse, where the states $1s\sigma_g$ and $2p\sigma_u$ are strongly coupled, one may alternatively consider the ionization process as occurring toward the corresponding field-dressed states. By including L_{elec} in the electronic Hamiltonian and diagonalizing the electronic Hamiltonian in the basis of the two states $|\phi_{R,g}\rangle$ and $|\phi_{R,u}\rangle$ one obtains the lowest dressed state

$$|\phi_{R,\text{low}}\rangle = M_g |\phi_{R,g}\rangle + M_u |\phi_{R,u}\rangle \quad (23)$$

(see, e.g., Ref [30] for explicit expressions of M_g and M_u). We can treat the ionization process as a transition toward this dressed state with a jump operator

$$C_h = \int d\vec{R} \sqrt{\Gamma_h(\vec{R})} (M_g |\phi_{R,g}\rangle + M_u |\phi_{R,u}\rangle) \langle \phi_{R,h}| \otimes |\vec{R}\rangle \langle \vec{R}|, \quad (24)$$

which now coherently feeds population into both the $1s\sigma_g$ and $2p\sigma_u$ states. We have applied simulations with both Eqs. (22) and (24), and find that the difference is very small, see Fig. 2.

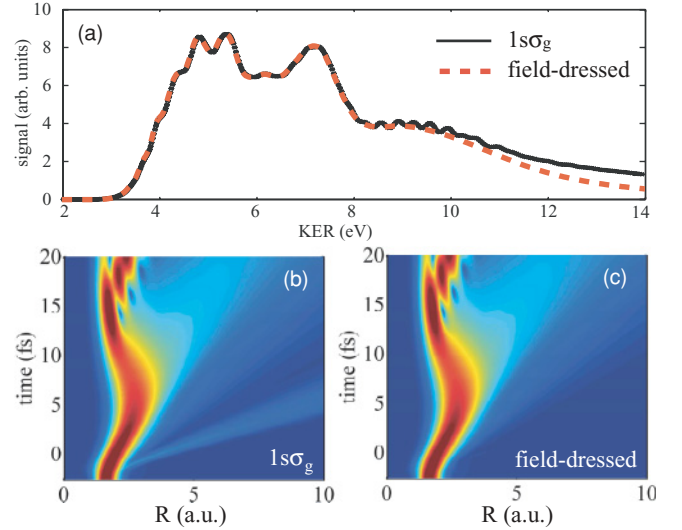


FIG. 2. (Color online) (a) Calculated KER spectra for pulses of $\lambda = 800$ nm, $\tau_{\text{FWHM}} = 40$ fs and $I = 6 \times 10^{13}$ W/cm² using both the $1s\sigma_g$ state [Eq. (22)] and the lowest field-dressed state [Eq. (24)] as initial state in H_2^+ (no focal volume averaging). (b) and (c) Total nuclear probability distribution in the H_2^+ system [i.e., $\sum_{a=g,u} |K_a(R, t)|^2$] given a first jump 3.8 fs prior to the peak of the pulse in the two different cases. The same logarithmic color scale is used in (a) and (b) for any discrepancy to be visible.

Apart from a weak and unphysically fast dissociating component contained in the wave function obtained with Eq. (22) there is no significant difference in the KER spectra obtained using the two approaches. When dealing with larger systems one might thus choose the simpler approach of Eq. (22) to avoid the diagonalization step.

The second ionization can occur either from the $1s\sigma_g$ state or from the $2p\sigma_u$ state, and the two pertaining jump operators are written as

$$C_g = \int d\vec{R} \sqrt{\Gamma_g(\vec{R})} |\phi_{R,c}\rangle \langle \phi_{R,g}| \otimes |\vec{R}\rangle \langle \vec{R}|, \quad (25)$$

$$C_u = \int d\vec{R} \sqrt{\Gamma_u(\vec{R})} |\phi_{R,c}\rangle \langle \phi_{R,u}| \otimes |\vec{R}\rangle \langle \vec{R}|. \quad (26)$$

Here $\Gamma_g(\vec{R})$ and $\Gamma_u(\vec{R})$ represent instantaneous ionization rates from the $1s\sigma_g$ and the $2p\sigma_u$ states, respectively. As for the first ionization we assume the static ionization rates, changing with the time-dependent strength of the field, applies. The static field rates for ionization of H_2^+ are available from Ref. [31].

To maintain the simplicity of the MCWP theory we choose to treat the second ionization step as a process occurring from the field-free electronic eigenstates Eqs. (25) and (26). A description based upon the dressed states would introduce coherent contributions to the ionization, described by superposition jump operators of the form ($C = C_g \pm C_u$). The difference between a coherent and an incoherent treatment of the ionization from the pair of H_2^+ states is, however, washed out by the rapid phase evolution and the sampling over the random times at which the jumps occur. Based on the good agreement with the experimental results obtained, the choice of using Eqs. (25) and (26) seems a plausible one.

Once the Hamilton and jump operators are known, the total non-Hermitian operator (5) is written as

$$H = H_s - \frac{i}{2} \sum_{a=h,g,u} \int d\vec{R} \Gamma_a(R) |\phi_{Ra}\rangle \langle \phi_{Ra}| \otimes |\vec{R}\rangle \langle \vec{R}|, \quad (27)$$

and the MCWP calculations can be performed. Figure 3 provides an overview of the simulation procedure (see points 1–4 in Sec. III A).

C. Calculation strategy

1. Simulations

Starting in the electronic and vibrational ground state of H_2 the time evolution operator is applied and the drop in norm dP associated with the non-Hermitian part of the Hamiltonian, Eq. (27), is determined. A random number ϵ between zero and unity is drawn and depending on the values of this number compared to the drop in the norm, we either renormalize or jump $|\Psi\rangle \rightarrow C_h|\Psi\rangle$ and subsequently renormalize. The time where this first jump occurs in a given simulation is denoted T_1 . Time evolution proceeds in the H_2^+ system until the draw of a random number determines that a second jump occurs. We denote this transition time T_2 . In the H_2^+ system, the two

jump possibilities $|\Psi\rangle \rightarrow C_g|\Psi\rangle$ and $|\Psi\rangle \rightarrow C_u|\Psi\rangle$ are distinguished by different probabilities

$$dP_g/dP = \frac{\langle \Psi | C_g^\dagger C_g | \Psi \rangle}{\langle \Psi | C_g^\dagger C_g + C_u^\dagger C_u | \Psi \rangle}, \quad (28)$$

$$dP_u/dP = \frac{\langle \Psi | C_u^\dagger C_u | \Psi \rangle}{\langle \Psi | C_g^\dagger C_g + C_u^\dagger C_u | \Psi \rangle}. \quad (29)$$

After application of either C_g or C_u , the system is in the doubly ionized state and further propagation of the wave function is not necessary since all the information concerning the kinetic-energy distribution of the outgoing fragments is already present in the wave function $K_c(R,t)$ through a projection onto the energy eigenstates of the Coulomb problem

$$E_a^{\text{KER}}(T_1, T_2) = \left| \int K_E(R) K_c(R,t) dR \right|^2. \quad (30)$$

Here $K_E(R)$ is the energy normalized Coulomb wave of energy E . If the calculation is performed in a box of size R_{max} a factor of $\sqrt{\frac{R_{\text{max}}\mu}{\pi k}}$, $k = \sqrt{2\mu E}$ is to be multiplied on the wave function to obtain the correct energy normalization [32].

2. Deterministic sampling

When propagating the wave function with the MCWP method the initial state is the same in all cases, and the evolution of the wave function up until the first jump will not differ in different realizations. Likewise, the evolution in the coupled $1s\sigma_g-2p\sigma_u$ system will be identical given a specific time for the first jump. These facts can be utilized to dramatically reduce the amount of calculations and replace the stochastic part of the approach by a deterministic weighted average.

Starting in the H_2 ground state, a single wave function is propagated in the H_2 system using the non-Hermitian Hamiltonian until the end of the pulse without renormalization. This leads to a nuclear wave function as a function of time with a continuously decreasing squared norm $N_h(t)$. One can show that the distribution of times for the first jump T_1 , following the procedure outlined previously for each short time step is given by

$$P_h(T_1) = -\frac{d}{dt} N_h(t)|_{t=T_1}. \quad (31)$$

This implies that we can sample the effect of the first jumps as a weighted sum over histories, with jump times T_1 belonging to an equidistant grid with weight factor $P_h(T_1)$. At every one of these sample times, the jump operator C_h is applied to the no-jump wave function, and the starting conditions for propagation in the singly ionized H_2^+ state is obtained for every T_1 free from stochastic sampling errors and with only one initial propagation in the H_2 system.

Concerning the evolution in the H_2^+ system similar simplifications can be made. Unfortunately, here the initial conditions are not identical in all runs and the evolution in the no-jump case must be done for every possible entering time T_1 . The drop in squared norm of both the $1s\sigma_g$ state $N_g(t)$ and the

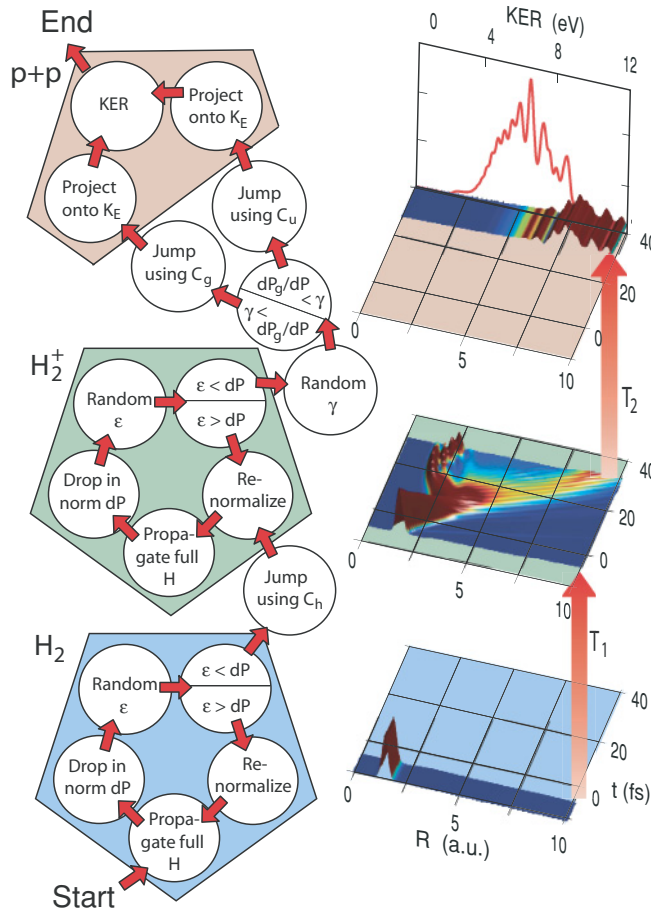


FIG. 3. (Color online) Overview of the calculational strategy for dissociative double ionization of H_2 with the MCWP approach. Each circle to the left corresponds to a computational task. The drawing of random numbers leads to a variety in the outcome of different realizations. A possible realization is illustrated to the right.

$2p\sigma_u$ state $N_u(t)$ now determines the conditional probability of a second jump at time T_2 given an initial jump at time T_1

$$P_{gu}(T_2 | T_1) = -\frac{d}{dt}[N_g(t) + N_u(t)]|_{t=T_2}. \quad (32)$$

To sample the effect of the second jump, where either C_g or C_u is randomly applied in accordance with Eqs. (28) and (29), both components are simply evaluated separately with these probabilities as deterministic weight factors.

In the doubly ionized state, the KER spectrum is determined for all values of the two jump times T_1 and T_2 and using both a C_g and a C_u jump. Following the previous discussion, the final result is obtained by evaluating the weighted summation

$$E_{\text{tot}}^{\text{KER}} = \sum_{T_1, T_2} P_h(T_1) P_{gu}(T_2 | T_1) \times \left[\sum_{a=g, u} P(a | \{T_1, T_2\}) E_a^{\text{KER}}(T_1, T_2) \right], \quad (33)$$

where $P(a | \{T_1, T_2\}) = dP_a/dP$ [Eqs. (28) and (29)] evaluated for wave functions with the specific jump times T_1 and T_2 . A very dense time grid is used for our numerical propagation of the Schrödinger equation, but it is not necessary to determine all possible contributions to $E_g^{\text{KER}}(T_1, T_2)$ and $E_u^{\text{KER}}(T_1, T_2)$ with the same time resolution. Indeed, the full calculation of a molecule exposed to an intense laser pulse of 40 fs and 800 nm reduces to one propagation in the H_2 system, and approximately 15 propagations in the H_2^+ system with different initial times suffice for convergence of the results. After completing the H_2 evolution, the remaining calculations can be made in parallel. Each of the propagations takes approximately 15 min on an AMD/Opteron 2.6 GHz processor and hence the total cost in CPU time for obtaining a KER spectrum for one intensity component of the field is only a few hours.

V. RESULTS

Using the MCWP technique the results of several different experiments on the double ionization of H_2 (D_2) in short intense laser pulses can be reproduced. Many of these experiments are discussed in [11] including a detailed analysis of the physical insight gained. In this paper, the results on H_2 in pulses of 800 nm, 1.0×10^{14} W/cm², and a Gaussian pulse of 40 fs in duration (FWHM) is given as an example to emphasize the importance of the different elements in the MCWP technique. The Keldysh parameter γ [33] for both the first and the second ionization lies for these pulses in the range 1.17–1.26, depending on the internuclear separation at the time of the ionization event, partly supporting the tunneling picture adapted in the use of static field ionization rates. The same results are briefly discussed in Ref. [10].

Starting in the electronic and nuclear ground state of H_2 , the evolution of the neutral molecule is the first to be calculated. The results are given in Fig. 4 using the peak of the pulse as the origin of the time axis. Panel (a) gives the nonnormalized probability density $|\tilde{K}_h(R, t)|^2$ in the electronic state ($1s\sigma_g$)² as a function of both internuclear separation and time. The tilde on the wave function indicates that the wave function is not normalized. Integrating over all possible separations, the squared norm is obtained and plotted in panel (b). As seen

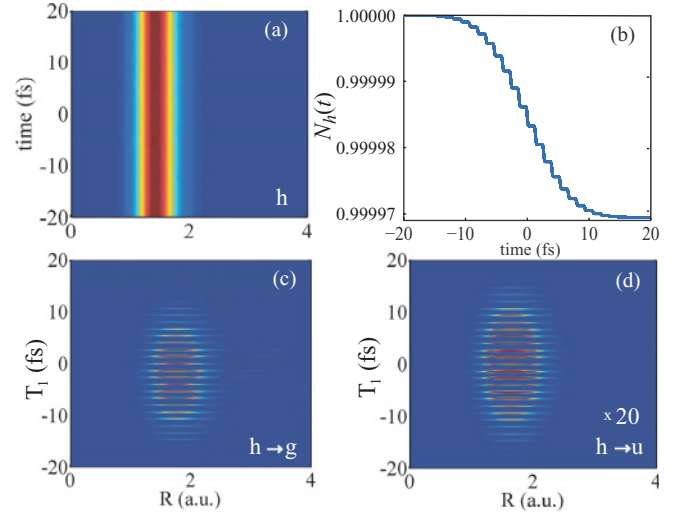


FIG. 4. (Color online) MCWP realization for H_2 exposed to pulses of 800 nm, 40 fs, and 6×10^{13} W/cm². (a) Nonnormalized population density in the ($1s\sigma_g$)² state $|\tilde{K}_h(R, t)|^2$ and (b) the integrated squared norm. (c) The amount of population entering the $1s\sigma_g$ state $|M_g \sqrt{\Gamma_h(R)} \tilde{K}_h(R, T_1)|^2$ and (d) the $2p\sigma_u$ state $|M_u \sqrt{\Gamma_h(R)} \tilde{K}_h(R, T_1)|^2$ as a function of the first jump time T_1 .

from the norm, only approximately 0.002% of the molecules undergo ionization at the intensity 6×10^{13} W/cm². Together with the initial condition this results in almost no changes in the probability distribution of panel (a) as a function of time. However, dynamics do indeed appear as seen from panels (c) and (d), which show the probability density entering the $1s\sigma_g$ and $2p\sigma_u$ states, respectively. More precisely, the state of panel (a) is projected using the jump operator C_h of Eq. (24), and the result is normalized and weighted by the jump probability $P_h(T_1)$ for all values of T_1 and the population density is plotted as a function of this parameter. Since the jump probability can be shown to equal $P_h(T_1) = \Gamma_h(R) |\tilde{K}_h(R, T_1)|^2 dt$ and the normalization constant is $1/\tilde{K}_h(R, T_1)$, the populations entering the $1s\sigma_g$ and the $2p\sigma_u$ states are $|M_g \sqrt{\Gamma_h(R)} \tilde{K}_h(R, T_1)|^2$ and $|M_u \sqrt{\Gamma_h(R)} \tilde{K}_h(R, T_1)|^2$, respectively, where M_g and M_u are defined in Eq. (23). The population is seen to be transferred mostly at the extrema of the external field with maximum at the peak of the pulse just as expected. To the careful eye it is seen that the density is shifted a little toward larger internuclear distances reflecting the tendency in the rate Γ_h as a function of internuclear distance R .

Even though the density distribution entering the singly ionized state is shifted in R compared to the equilibrium distance in the ground state of H_2 , it is still centered at relatively small internuclear distances (~ 1.5 a.u.). Since the equilibrium distance in H_2^+ is 2.0 a.u. this induces nuclear dynamics as seen from Fig. 5(a) showing the population density in the $1s\sigma_g$ state $|\tilde{K}_g(R, t)|^2$ under the assumption that the first ionization occurs at $T_1 = -13$ fs. The characteristic vibrational time scale of 15 fs in the $1s\sigma_g$ state is reflected in the nuclear dynamics. Figure 5(b) shows the population density in the $2p\sigma_u$ state $|\tilde{K}_u(R, t)|^2$, using the same initial conditions and here population transfer from the $1s\sigma_g$ state is seen due to the strong dipole coupling. The $2p\sigma_u$ state is dissociative and the wave function spreads out.

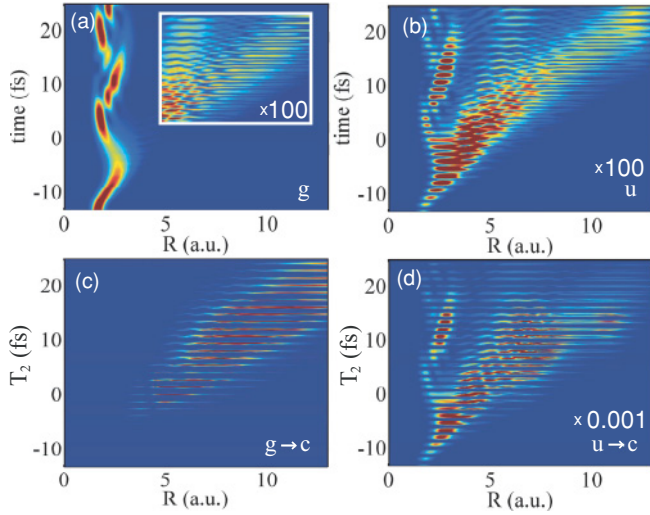


FIG. 5. (Color online) MCWP realization for H_2 exposed to pulses of 800 nm, 40 fs, and 6×10^{13} W/cm 2 . To illustrate the dynamics, the first ionization event is restricted to one specific time $T_1 = -13$ fs. (a) Nonnormalized population density in the $1s\sigma_g$ state $|\tilde{K}_g(R,t)|^2$ and (b) 100 times the nonnormalized population density in the $2p\sigma_u$ state $|\tilde{K}_u(R,t)|^2$ using the same color scale. (c) The amount of the population entering the doubly ionized state from the $1s\sigma_g$ state $|\sqrt{\Gamma_g(R)} \tilde{K}_g(R, T_2)|^2$ as a function of the second jump time T_2 . (d) The population entering the doubly ionized state from the $2p\sigma_u$ state $|\sqrt{\Gamma_u(R)} \tilde{K}_u(R, T_2)|^2$ multiplied by 0.001, on the same color scale as (c).

In addition to modulations as a function of time, $|\tilde{K}_u(R,t)|^2$ shows modulations as a function of internuclear separation as well due to the structure of the ionization rate $\Gamma_u(R)$ at large distances [31]. The evolution shown is calculated in the no-jump case, but the dynamics is still affected by the ionization rate, a fact referred to as the Lochfrass effect [34,35]. In regions of a high ionization rate, the probability density is lowered, while it is raised in regions of low ionization rate. The same effect is responsible for the population of “dark states” in quantum optics (cf. the discussion in [12]).

The modulation in the population density is also seen in the states entering the doubly ionized space. Figures 5(c) and 5(d) show the probability density right after the second jump from $1s\sigma_g$ and $2p\sigma_u$, respectively. That is $|\sqrt{\Gamma_g(R)} \tilde{K}_g(R, T_2)|^2$ and $|\sqrt{\Gamma_u(R)} \tilde{K}_u(R, T_2)|^2$. In the $2p\sigma_u$ case a clear enhancement of the probability density is seen for large internuclear separations and charge resonance enhanced ionization (CREI) [31,36] at $R=7$ a.u. and $R=11$ a.u. gives two separate structures. Turning to the $1s\sigma_g$ case, the same enhancement at large separations is observed. This occurs despite the fact that the wave function in the $1s\sigma_g$ state has almost no weight in this region. The population transferred, accordingly, corresponds to molecules that first couple to the $2p\sigma_u$ potential curve, dissociate, and later couple back to the $1s\sigma_g$ state [see the right corner of panel (a), where the population density is multiplied by 100]. Due to this more complicated scheme involving two transitions in the singly ionized space and a lower ionization rate, the amount of population transferred in this way is down by a factor of 1000 compared to the amount transferred directly from the $2p\sigma_u$ state.

Having determined the probability density right after the second jump a projection onto repulsive continuum Coulomb states will give the KER spectra. Figure 6(a) shows the result summed over all possible second jump times T_2 , but restricted to one specific first jump time T_1 for four different values of T_1 . The spectrum is clearly different for different T_1 's. Hence theoretical models attempting to describe dissociative double ionization using only one specific starting time in the single ionized state will most probably fail to predict future experiments. To see how much the individual jump times contribute to the overall spectrum Fig. 6(b) shows integrated jump probabilities. The dotted bars indicate the probabilities of a first ionization $P_h(T_1)$ at time T_1 and show, as expected, to be centered around the peak of the pulse. The gray bars, on the other hand, show the probability of a second ionization at any time given a first ionization at time T_1

$$P_2(T_1) = \int_{T_1}^{\infty} P_{gu}(t|T_1) dt. \quad (34)$$

The maximum in ionization probability is here at $T_1 = 15$ fs, allowing the wave function to reach regions of high rates at maximum intensity. Multiplying the two probabilities gives the weight of the individual KER spectra and peaks at -3 fs as indicated by the black bars. This result shows that if the dissociative double-ionization process in H_2 was modeled by initiating the propagation in the H_2^+ system at $T_1 = -3$ fs, a good agreement might accidentally occur. However, since many different jump times contribute significantly, this is far from certain, and perfect agreement can only be obtained by including them all.

Including all possible jump times is not the only summation required to obtain the correct KER spectrum. Using short intense laser pulses the extent of the molecular sample is most often larger than the waist of the pulse and a focal volume averaging is necessary [37]. Figure 7(a) shows the total KER spectra of four different intensities, which after averaging over a pulse of 7×10^{13} W/cm 2 in center peak

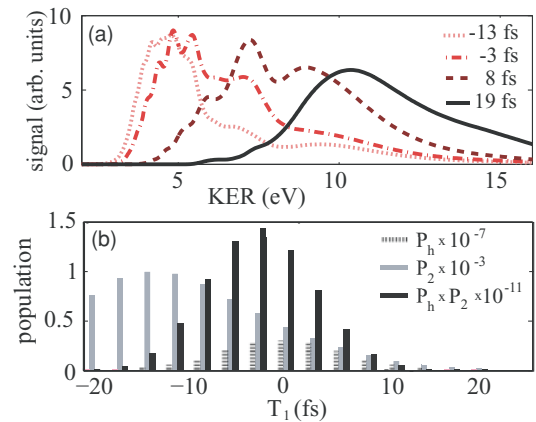


FIG. 6. (Color online) (a) The KER spectra obtained if restricted to four different values of the first jump time, T_1 . (b) The amount of population entering the singly ionized state (dotted bar). The amount of population leaving the singly ionized state if entered at T_1 (gray bar). The product of the two giving the weight of the different initial jump times in the total KER spectrum (black bar). Pulses of 800 nm, 40 fs, and 6×10^{13} W/cm 2 are used.

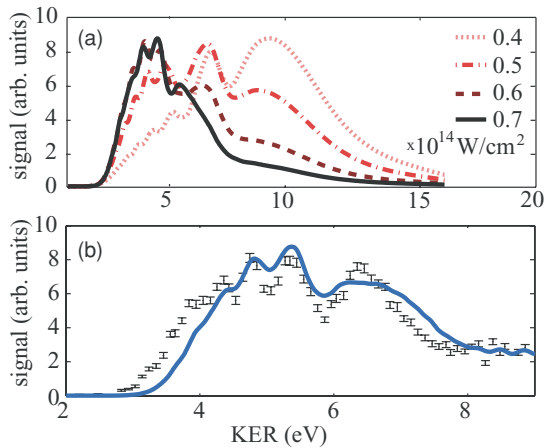


FIG. 7. (Color online) (a) The KER spectrum calculated at four different intensities (no focal volume averaging). (b) The KER spectrum after focal volume averaging (full line) and experimental results [6] (points) using pulses of 800 nm and 40 fs. The peak intensity in the experiments is 1×10^{14} W/cm² and a peak intensity of 7×10^{13} W/cm² is used in the simulations.

intensity leads to the total spectrum given in Fig. 7(b). A comparison to experiments [6] can now be performed and as seen from Fig. 7(b) the agreement is very convincing. The experiments were carried out at the same pulse duration and wavelength as the calculations, however, at a slightly higher peak intensity (1×10^{14} W/cm²). Given that the uncertainty in peak laser intensity is stated to be $\sim 10\%$ [6], we consider the agreement obtained very good.

VI. CONCLUSION

Using the MCWP technique we have presented an approach to study dissociative multiple-ionization processes in diatomic molecules as a system-environment interaction problem. The system of concern is the molecule, while the environment

is associated with the electrons escaping the molecular ion, and the method is formally equivalent to solving the master equation for this problem. For systems including spatial motion the Hilbert space is, however, too large for a direct solution of the master equation and instead the density matrix is replaced by an ensemble of individual state vectors, which are evolved stochastically with time. By propagating an ensemble of pure-state wave function subject to a non-Hermitian Hamiltonian operator, the drop in norm in every time step is determined and in combination with a random number generator this leads to quantum jumps among the different charge states at different instances of time. Physically, these jumps can be interpreted as hypothetical measurements of the escaping electrons effectively removing them from the quantum description and projecting the remaining molecular system on the charge state corresponding to the measurement outcome. The technique relies on the Born-Markov approximation and assumes a weak interaction and a rapid spread of quantum excitation of the environment degrees of freedom (i.e., electron recapture is not a significant process in the ionization dynamics).

The MCWP technique is relatively simple to implement and runs at a low computationally cost and hence the technique is a very good candidate for calculations on larger molecules than H₂ or in other pulse regimes. For example, N₂ in extreme ultraviolet pulses [38]. As long as the electronic energies and dipole moment functions are known and the ionization rates can be determined, the MCWP technique offers insight into the dynamics of ionization events and makes it possible to both predict future experiments and address physical explanations. A detailed comparison with a range of experimental data available for H₂ and D₂ [6,39,40] can be found in [11].

ACKNOWLEDGMENTS

This work was supported by the Danish Research Agency (Grant No. 2117-05-0081).

-
- [1] S. Chelkowski, A. D. Bandrauk, A. Staudte, and P. B. Corkum, *Phys. Rev. A* **76**, 013405 (2007).
 - [2] F. Légaré, I. V. Litvinyuk, P. W. Dooley, F. Quéré, A. D. Bandrauk, D. M. Villeneuve, and P. B. Corkum, *Phys. Rev. Lett.* **91**, 093002 (2003).
 - [3] A. Rudenko, B. Feuerstein, K. Zrost, V. L. B. de Jesus, T. Ergler, C. Dimopoulou, C. D. Schroter, R. Moshhammer, and J. Ullrich, *J. Phys. B* **38**, 487 (2005).
 - [4] G. N. Gibson, M. Li, C. Guo, and J. Neira, *Phys. Rev. Lett.* **79**, 2022 (1997).
 - [5] M. Vafaee, *Phys. Rev. A* **78**, 023410 (2008).
 - [6] A. Staudte *et al.*, *Phys. Rev. Lett.* **98**, 073003 (2007).
 - [7] I. D. Williams *et al.*, *J. Phys. B* **33**, 2743 (2000).
 - [8] D. Pavičić, A. Kiess, T. W. Hänsch, and H. Figger, *Phys. Rev. Lett.* **94**, 163002 (2005).
 - [9] B. D. Esry, A. M. Saylor, P. Q. Wang, K. D. Carnes, and I. Ben Itzhak, *Phys. Rev. Lett.* **97**, 013003 (2006).
 - [10] H. A. Leth, L. B. Madsen, and K. Mølmer, *Phys. Rev. Lett.* **103**, 183601 (2009).
 - [11] H. A. Leth, L. B. Madsen, and K. Mølmer, *Phys. Rev. A* **81**, 053410 (2010).
 - [12] J. Dalibard, Y. Castin, and K. Mølmer, *Phys. Rev. Lett.* **68**, 580 (1992).
 - [13] H. J. Carmichael, *An Open Systems Approach to Quantum Optics* (Springer-Verlag, Berlin Heidelberg, 1993).
 - [14] K. Mølmer, Y. Castin, and J. Dalibard, *J. Opt. Soc. Am. B* **10**, 524 (1993).
 - [15] B. Wolfseder, L. Seidner, G. S. W. Domcke, M. Seel, S. Engleitner, and W. Zinth, *Chem. Phys.* **233**, 323 (1998).
 - [16] S. Li and H. Guo, *J. Chem. Phys.* **117**, 4499 (2002).
 - [17] R. Dum, P. Zoller, and H. Ritsch, *Phys. Rev. A* **45**, 4879 (1992).
 - [18] K. Mølmer and Y. Castin, *Quant. Semicl. Optics* **8**, 49 (1996).
 - [19] Y. Castin and K. Mølmer, *Phys. Rev. Lett.* **74**, 3772 (1995).
 - [20] M. B. Plenio and P. L. Knight, *Rev. Mod. Phys.* **70**, 101 (1998).
 - [21] C. W. Gardiner and P. Zoller, *Quantum Noise* (Springer-Verlag, Berlin, 2000).
 - [22] V. Weisskopf and E. Wigner, *Z. Phys. A* **63**, 54 (1930).
 - [23] B. R. Mollow, *Phys. Rev. A* **12**, 1919 (1975).

- [24] D. Dimitrovski and L. B. Madsen, *Phys. Rev. A* **78**, 043424 (2008).
- [25] L. B. Madsen and D. Dimitrovski, *Phys. Rev. A* **78**, 023403 (2008).
- [26] O. Smirnova, M. Spanner, and M. Ivanov, *J. Phys. B* **39**, S307 (2006).
- [27] J. T. Lin and T. F. Jiang, *Phys. Rev. A* **63**, 013408 (2000).
- [28] F. Anis, T. Cackowski, and B. D. Esry, *J. Phys. B* **42**, 091001 (2009).
- [29] A. Saenz, *Phys. Rev. A* **66**, 063408 (2002).
- [30] H. Kono, Y. Sato, Y. Fujimura, and I. Kawata, *Laser Physics* **13**, 883 (2003).
- [31] M. Plummer and J. F. McCann, *J. Phys. B* **29**, 4625 (1996).
- [32] T.-Y. Wu and T. Ohmura, *Quantum Theory of Scattering* (Prentice-Hall, Englewood Cliffs, NJ, 1962).
- [33] L. V. Keldysh, *Sov. Phys. JETP* **20**, 1307 (1965).
- [34] E. Goll, G. Wunner, and A. Saenz, *Phys. Rev. Lett.* **97**, 103003 (2006).
- [35] T. Ergler, B. Feuerstein, A. Rudenko, K. Zrost, C. D. Schröter, R. Moshhammer, and J. Ullrich, *Phys. Rev. Lett.* **97**, 103004 (2006).
- [36] T. Zuo and A. D. Bandrauk, *Phys. Rev. A* **52**, R2511 (1995).
- [37] P. Wang, A. M. Saylor, K. D. Carnes, B. D. Esry, and I. Ben Itzhak, *Opt. Lett.* **30**, 664 (2005).
- [38] Y. H. Jiang *et al.*, *Phys. Rev. Lett.* **102**, 123002 (2009).
- [39] I. V. Litvinyuk, A. S. Alnaser, D. Comtois, D. Ray, A. T. Hasan, J.-C. Kieffer, and D. M. Villeneuve, *New J. Phys.* **10**, 083011 (2008).
- [40] T. Ergler, A. Rudenko, B. Feuerstein, K. Zrost, C. D. Schröter, R. Moshhammer, and J. Ullrich, *Phys. Rev. Lett.* **95**, 093001 (2005).